Article

# Current Transients in Single Nanoparticle Collision Events

Xiaoyin Xiao, Fu-Ren F. Fan, Jiping Zhou, and Allen J. Bard

*J. Am. Chem. Soc.*, **2008**, 130 (49), 16669-16677 • DOI: 10.1021/ja8051393 • Publication Date (Web): 14 November 2008



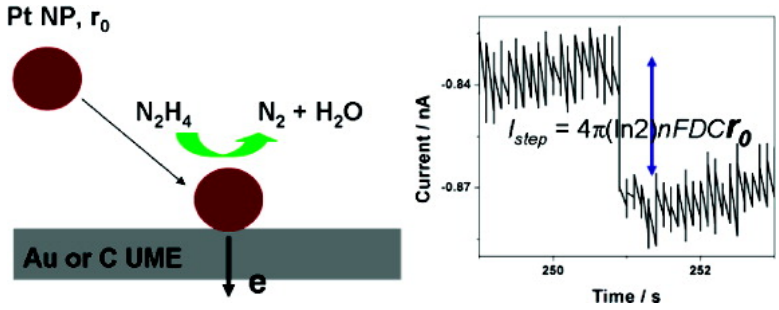


## More About This Article

Additional resources and features associated with this article are available within the HTML version:

- Supporting Information
- Access to high resolution figures
- Links to articles and content related to this article
- Copyright permission to reproduce figures and/or text from this article

View the Full Text HTML

J|A|C|S
ARTICLES

Published on Web 11/14/2008

# Current Transients in Single Nanoparticle Collision Events

Xiaoyin Xiao, Fu-Ren F. Fan, Jiping Zhou, and Allen J. Bard*

*Center for Electrochemistry, Department of Chemistry and Biochemistry, University of Texas at Austin, 1 University Station A5300, Austin, Texas 78712-0165*

Received July 3, 2008; E-mail: ajbard@mail.utexas.edu

***Abstract:*** Electrochemical hydrazine oxidation and proton reduction occur at a significantly higher rate at Pt than at Au or C electrodes. Thus, the collision and adhesion of a Pt particle on a less active Au or C electrode leads to a large current amplification by electrocatalysis at single nanoparticles (NPs). At low particle concentrations, the collision of Pt NPs was characterized by current transients composed of individual current profiles that rapidly attained a steady state, signaling single NP collisions. The characteristic steady-state current was used to estimate the particle size. The fluctuation in collision frequency with time indicates that the collision of NPs at the detector electrodes occurs in a statistically random manner, with the average frequency a function of particle concentration and diffusion coefficient. A longer term current decay in single current transients, as opposed to the expected steady-state behavior, was more pronounced for proton reduction than for hydrazine oxidation, revealing microscopic details of the nature of the particle interaction with the detector electrode and the kinetics of electrocatalysis at single NPs. The study of single NP collisions allows one to screen particle size distributions and estimate NP concentrations and diffusion coefficients.

## Introduction

Metal nanoparticles (MNPs) of sizes ranging from subnanometer to a few nanometers are of both fundamental and practical interest (e.g., in catalysis and biotechnology).[1−7] Because of their large surface-to-volume ratio, size-dependent optical properties, and high density of surface defects, these particles show unusual physical and chemical properties. MNPs are most frequently characterized by transmission electron microscopy (TEM) or by spectroscopic methods. [1−10]

In electrochemical studies, MNPs are usually immobilized on an inert supporting material to form an electrode and then their effect in electrocatalytic reactions, such as proton or oxygen reduction, is probed. In characterizing the electrocatalytic effect of MNPs in these experiments, the homogeneity of MNP size and shape plays a complicated role, as does their surface coverage on the supporting materials. One usually sees an average (ensemble) effect, and relating the activity to MNP properties is complicated by the effect of the surface coverage, total area, and particle distribution, as well as the interaction of particles with supporting materials. Thus, for example, there has been disagreement about the effect of particle size on electrocatalytic behavior. [11−13]

Characterization of electrodes at the single nanoparticle (NP) level is challenging, with relatively few experimental studies reported.[14−17] It has also been proposed that nanoelectrodes or MNP electrodes would find applications ranging from single-molecule detection to real-time imaging of cell exocytosis.[18−22] The size of these electrodes is comparable to the size of biological molecules and of ion channels in biological membranes. However, making electrodes at the nanometer scale is still technologically challenging. Moreover, at nanometer size the current generated at such electrodes is usually at picoampere levels, making measurements with good signal-to-noise levels

(1) Tian, N.; Zhou, Z. Y.; Sun, S. G.; Ding, Y.; Wang, Z. L. *Science* **2007**, *316*, 732–735.
(2) Narayanan, R.; El-Sayed, M. A. *Chimica OGGI-Chem Today* **2007**, *25*, 84–86. Narayanan, R.; El-Sayed, M. A. *J. Phys. Chem. B* **2005**, *109*, 12663–12676.
(3) Yang, J.; Lee, J. Y.; Too, H. P. *Anal. Chim. Acta* **2006**, *571*, 206–210.
(4) Bratlie, K. M.; Lee, H.; Komvopoulos, K.; Yang, P. D.; Somorjai, G. A. *Nano Lett.* **2007**, *7*, 3097–3101.
(5) Polsky, R.; Gill, R.; Kaganovsky, L.; Willner, I. *Anal. Chem.* **2006**, *78*, 2268–2271.
(6) Rosi, N. L.; Giljohann, D. A.; Thaxton, C. S.; Lytton-Jean, A. K. R.; Han, M. S.; Mirkin, C. A. *Science* **2006**, *312*, 1027–1030.
(7) Sonnichsen, C.; Reinhard, B. M.; Liphardt, J.; Alivisatos, A. P. *Nat. Biotechnol.* **2005**, *23*, 741–745.
(8) Solla-Gullon, J.; Lafuente, E.; Aldaz, A.; Martinez, M. T.; Feliu, J. M. *Electrochim. Acta* **2007**, *52*, 5582–5590.
(9) Haiss, W.; Thanh, N. T. K.; Aveyard, J.; Fernig, D. G. *Anal. Chem.* **2007**, *79*, 4215–4221.
(10) Jentys, A. *Phys. Chem. Chem. Phys.* **1999**, *1*, 4059–4063.
(11) Cherstiouk, O. V.; Simonov, P. A.; Savinova, E. R. *Electrochim. Acta* **2003**, *48*, 3851–3860.
(12) Antoine, O.; Bultel, Y.; Durand, R.; Ozil, P. *Electrochim. Acta* **1998**, *43*, 3681–3691.
(13) Rao, V.; Simonov, P. A.; Savinova, E. R.; Plaksin, G. V.; Cherepanova, S. V.; Kryukova, G. N.; Stimming, U. *J. Power Sources* **2005**, *145*, 178–187.
(14) Fan, F. R. F.; Bard, A. J. *Science* **1997**, *277*, 1791–1793. Tel-Vered, R.; Bard, A. J. *J. Phys. Chem. B* **2006**, *110*, 25279–25287.
(15) Chen, S. L.; Kucernak, A. *J. Phys. Chem. B* **2003**, *107*, 8392–8402.
(16) Krapf, D.; Wu, M. Y.; Smeets, R. M. M.; Zandbergen, H. W.; Dekker, C.; Lemay, S. G. *Nano Lett.* **2006**, *6*, 105–109.
(17) Meier, J.; Schiotz, J.; Liu, P.; Norskov, J. K.; Stimming, U. *Chem. Phys. Lett.* **2004**, *390*, 440–444.
(18) Wightman, R. M. *Science* **2006**, *311*, 1570–1574.
(19) Quinn, B. M.; Lemay, S. G. *Adv. Mater.* **2006**, *18*, 855–859.
(20) Staal, R. G. W.; Mosharov, E. V.; Sulzer, D. *Nature Neurosci.* **2004**, *7*, 341–346.
(21) Wu, W. Z.; Huang, W. H.; Wang, W.; Wang, Z. L.; Cheng, J. K.; Xu, T.; Zhang, R. Y.; Chen, Y.; Liut, J. *J. Am. Chem. Soc.* **2005**, *127*, 8914–8915.
(22) Amemiya, S.; Guo, J. D.; Xiong, H.; Gross, D. A. *Anal. Bioanal. Chem.* **2006**, *386*, 458–471.

  

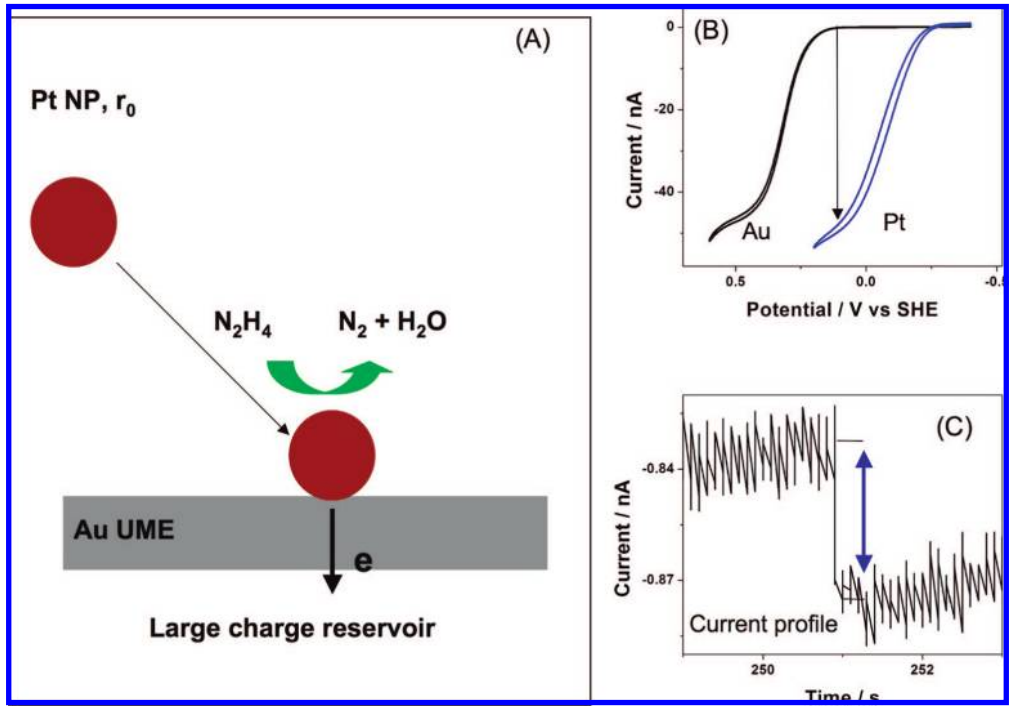


***Figure 1.*** Principle of single nanoparticle collision experiments. (A) Scheme of single NP collision at the Au UME surface; the reaction is switched on when the particle is in contact with the detection electrode. (B) Current amplification: tuning the hydrazine oxidation rate between Au and Pt UMEs. Scan rate, 50 mV/s; electrolyte, 10 mM hydrazine + 50 mM PBS buffer, pH ~7.5. (C) Representative current profile observed in a single NP collision event.

challenging. A variety of analytical tools have been developed to determine MNP size and size distributions, e.g., electron microscopy, scanning probe microscopy, UV−visible spectroscopy, surface plasma resonance, mass spectrometry, dynamic light scattering, and X-ray absorption spectroscopy (XRD and EXAFS). Among these, transmission electron microscopy (TEM) is common and widely used to determine the size of MNPs of a few nanometers in diameter by casting on a carbon grid. Here we demonstrate a straightforward and specific electrochemical method that is able to screen the MNP sizes in a liquid solution and also provide a platform for the study of the kinetics of electrocatalysis at single MNPs.

## Principles and Experimental Criteria

In a previous communication we described the detection of single MNP collisions through electrocatalytic amplification.[23] Briefly, a heterogeneous electron-transfer reaction is selected that occurs sluggishly at a given detector electrode material, e.g., C, but takes place at the MNPs when they collide and stick to the electrode. Once the MNP is in contact with the detector electrode, electrons flow into or out of the MNP, maintaining the catalytic reactions at the MNP surface (Figure 1A). The particle collisions will thus lead to individual current steps (Figure 1C). The amplitude of the current steps at the mass-transfer limiting current generated at individual spherical MNPs in contact with a planar electrode is given by

$$I = 4\pi(\ln 2)nFDCr \qquad (1)$$

where $D$ is the diffusion coefficient of reactants at concentration of $C$, and $r$ is the radius of a single MNP. This equation differs from that for a spherical ultramicroelectrode (UME) by the ln 2 term, which accounts for blocking of the diffusion path to the MNP by the supporting planar surface.[24,25] Clearly, the particle size, or radius $r$, is proportional to the catalytic current recorded at a given concentration $C$ of the reactants, assuming that the diffusion coefficient $D$ is kept constant in a certain concentration range of reactants and supporting electrolytes, which are mostly less than 100 mM in our experiments.

To observe such individual current steps for single MNP collisions, one must first amplify the current by selecting a catalytic reaction. First, the reaction rate at the MNP must be significantly faster than that at the substrate within a certain potential range, e.g., proton reduction at Pt vs C. Second, the catalytic reaction should occur under diffusion-controlled conditions with negligible kinetic influence, where the current is proportional to the size of MNPs, i.e., eq 1 applies. Since the heterogeneous kinetics of electrocatalysis at MNPs may be a function of their geometry and the capping agent, it is useful to minimize these effects by biasing the electrode at a potential where the diffusion-limited current at the MNP can be attained. Finally, the reactant should be at a high concentration and have a large diffusion coefficient so that a large enough current, well above the detection limit, i.e., of the order of tens of picoamperes or more, is obtained.

In addition to proton reduction, we have examined reactions such as oxygen reduction, oxidation of small organic molecules, i.e., methanol and formic acid, oxidation or reduction of hydrogen peroxide, and hydrazine oxidation at Pt, Au, and C microelectrodes. All of these reactions show potential differences in their electrocatalytic response among these electrodes. However, the amount of current from oxygen reduction is limited by its poor solubility, and thus low concentration, in water. The oxidation of small organic molecules, such as

(23) Xiao, X. Y.; Bard, A. J. *J. Am. Chem. Soc.* **2007**, *129*, 9610–9612.

(24) Bard, A. J.; Faulkner, L. R. *Electrochemcial Methods, Fundamentals and Applications*, 2nd ed.; John Wiley & Sons: New York, 2001.

(25) Bobbert, P. A.; Wind, M.; Vlieger, M. *J. Physica* **1987**, *141A*, 58–72.

methanol and formic acid, leads to poisoning of the surface by adsorbed intermediates, like CO, which limits and causes instability of the oxidation current. The use of $H_2O_2$ is perturbed by the heterogeneous catalytic decomposition of hydrogen peroxide, and gas bubbles are generated when Pt MNPs are injected into a hydrogen peroxide test solution. Hydrazine oxidation and proton reduction show distinguishable catalytic behavior among Pt, Au, and C electrodes and yield reproducible responses in certain pH regions. Figure 1B, as an example, shows that hydrazine oxidation gives rise to a steady-state limiting current at a Au UME at potentials above 0.4 V in a pH 7.5 phosphate buffer, while the potential for oxidation is shifted by about −0.5 V at a Pt UME. Such a shift would lead to a potential window that is large enough to tune the reaction rate at Pt to be significantly larger than that at Au. The steady-state limiting current is about 50 nA for 10 mM hydrazine and 75 nA for 15 mM hydrazine at pH 7.5 at an UME with a radius of 5 $\mu$m.

The individual stepwise current profiles (Figure 1C) correspond to single particle collision events and can be used to determine particle size, as described below. Such a current profile represents a single event of MNP collision and adhesion at the detector electrode before and after it switches on eletrocatalytic hydrazine oxidation at the particle surface. The current profile resembles the ones recorded at UMEs, indicating that a steady-state current at this MNP has been achieved. The amplitude of the current steps is a function of the particle size, as illustrated by eq 1. Alternatively, we can obtain the particle sizes by proportioning their currents to the limiting current recorded at a Pt UME in the same test electrolyte, with the size of Pt UME known. To evaluate the particle size distribution, we controlled the particle collision frequency by injecting very dilute Pt colloidal solutions into the test solution containing hydrazine and PBS buffer electrolyte. The well-separated current profiles signaled individual single MNP collision events.

## Experimental Section

**Preparation and Characterization of Pt Nanoparticles.** The Pt NP solutions were prepared through reduction of Pt precursors, $H_2PtCl_6$ or $K_2PtCl_4$, by sodium borohydride ($NaBH_4$) in the presence of sodium citrate.[3] Briefly, 40 mL of 2 mM $H_2PtCl_6$ (99.9%, Alfa Aesar) was mixed with 28 mg of sodium citrate (99+%, Aldrich), followed by dropwise addition of fresh sodium borohydride solution (99%, Aldrich) under vigorous magnetic stirring. The concentration of sodium borohydride was varied from 56 to 500 mM to control the particle size, and the solution was stirred for 30 min. The NP solution prepared with $H_2PtCl_6$ had a relatively narrow size distribution of around 3.2−5.3 nm in diameter, depending on the concentration of $NaBH_4$ injected, as determined by TEM. A Pt NP solution with particle sizes distributed around 3.6 nm was mainly used in the described particle collision experiments. These colloidal solutions were stable for a few months in the synthesis solution. Reduction of $K_2PtCl_4$ by $NaBH_4$ led to very small NPs, around 1.3 nm in diameter, or particle aggregates. The particle aggregates were star-shaped, with sizes ranging from 13 to 25 nm. Both of these colloidal solutions were not stable. Pt particle solutions were also prepared through hydrogen reduction of $K_2PtCl_4$ in the presence of potassium oxalate. In this preparation, the Pt particles have better crystallinity, but the particle sizes are widely distributed between 5 and 16 nm.

The NP concentration was usually calculated from the concentration of Pt precursor divided by the average number of Pt atoms contained in each particle. For example, a 3.6 nm Pt particle is assumed to contain ~1400 Pt atoms;[10] therefore, the Pt particle concentration is 1400 times smaller than that of the Pt precursor. We have confirmed by ICP-MS that the loss of Pt is negligible for the freshly prepared colloidal solution. The decrease of the Pt concentration by <5% is possibly due to a small amount of adhesion of the Pt particles to the magnetic stirring bar and the glass walls.

TEM was used to determine the particle sizes. To space the Pt particles far apart on the TEM grids, we immersed the TEM grids overnight into Pt colloidal synthesis solution diluted about 20 times with water, removed them from the colloidal solution vertically, and thoroughly rinsed them with water by immersion. The carbon films of the TEM grids were usually dry after rinsing, since the film was still sufficiently hydrophobic. If there was a water droplet left, we removed it immediately by contacting it with a piece of powder-free paper. Using this procedure, we were able to minimize the aggregation of the MNPs on the grid surface, allowing us to determine whether the as-prepared colloidal solution had particle aggregates. TEM samples prepared by drop-casting were used for comparison. TEM images were obtained using a JEOL 2010F transmission electron microscope (JEOL Ltd.). The TEM resolution for a point image was 0.194 nm. The TEM grids were carbon films supported on 200 mesh copper (Electron Microscope Sciences).

**Ultramicroelectrode Preparation and Modification with Self-Assembled Monolayers (SAMs).** UMEs (10 $\mu$m in diameter C, Au, and Pt; 25 $\mu$m in diameter Au and Pt) were prepared with carbon fiber, Au, and Pt microwires into molten soft glass. After the metal wire was connected to a Ni−Cr lead with silver epoxy, the electrode was polished finally with 0.05 $\mu$m alumina until a mirror surface was obtained. The projected surface area and the quality of UMEs were determined by voltammetry of ferrocene/methanol oxidation in an aqueous solution. Before each use, the electrode was polished with 0.3 and 0.05 $\mu$m $Al_2O_3$ powder. Modification of Au UMEs with SAMs of cystamine or 3-mercaptopropionic acid was followed by immersing the cleaned Au UMEs into ethanol solutions of the SAMs overnight. Oxidative treatment of C UMEs was carried out by immersing the cleaned C UMEs into freshly prepared piranha solution for about 1 min (piranha solution is 3:1 v/v concentrated sulfuric acid to hydrogen peroxide). [*Extreme* **caution** *should be used when handling piranha solution.*]

**Recording Single Nanoparticle Collisions.** Cyclic voltammetry and chronoamperometry were performed with a three-electrode cell containing about 50 mL of electrolyte, controlled by an electrochemical workstation (CH Instruments, Austin, TX, model 660). A carbon rod was used as the counter electrode, and a stainless steel wire coated with polypyrrole was used as the reference electrode.[26] The electrode potential was calibrated against a standard Ag/AgCl reference electrode and rescaled to yield potentials vs the standard hydrogen electrode (SHE). The electrochemical cell was maintained in a Faraday cage. Current transients were usually recorded at a data acquisition rate of 10 ms, unless noted otherwise, where a higher temporal resolution of 1 ms or below was used. Before injection of the Pt colloidal solution, the UME was subjected to a few potential cycles to clean the surface and was then held at the potential where the background current was <300 pA. Noise would appear when the Faraday cage was opened for MNP injection. After closing the cage, the cell was maintained under an Ar atmosphere. The currents generated by MNP collisions could be easily distinguished from the background noise at the amplification levels employed when the Faraday cage door was closed.

The current was recorded vs time before and after the Pt colloidal solution was injected. The colloidal solution was injected into the test electrolyte while the solution was bubbled with Ar for about 10 s. This procedure quickly distributed the Pt NPs uniformly in the whole test electrolyte but produced higher noise levels during this period.

## Results and Discussion

In the following two sections, we focus on hydrazine oxidation and proton reduction as the indicator reactions for

(26) Ghilane, J.; Hapiot, P.; Bard, A. J. *Anal. Chem.* **2006**, *78*, 6868–6872.

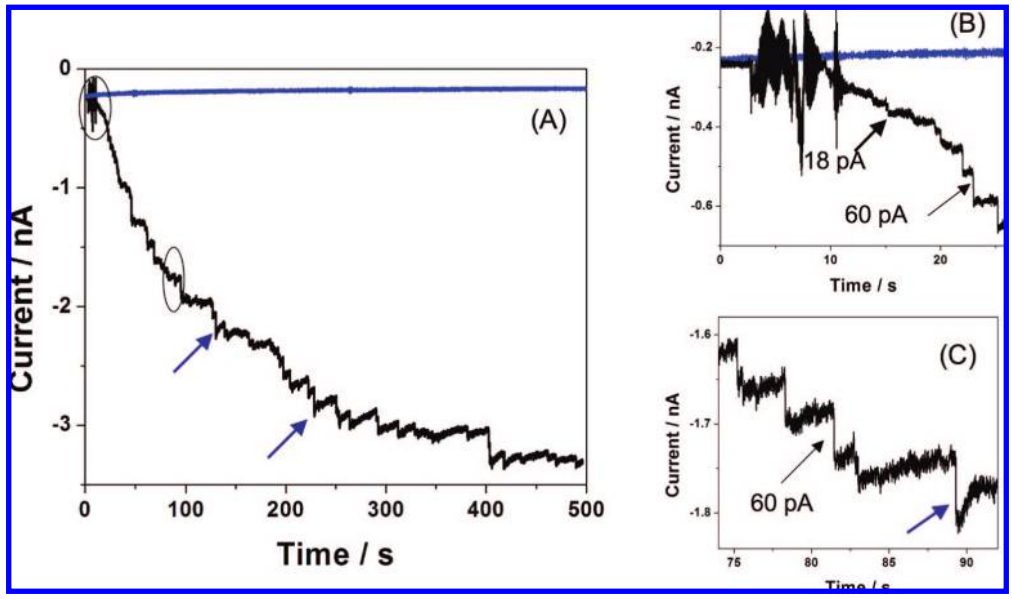


***Figure 2.*** (A) Current transient recorded before and after Pt particle solution was injected. (B) Zoom of the initial part of (A), and (C) the intermediate part. Colloidal solution: ~36 pM Pt nanoparticle solution; particle size, ~3.6 nm; 10 $\mu$m Au UME; 15 mM hydrazine + 50 mM PBS buffer, pH ~7.5. The black arrows point to peak current and the blue arrows to the long transient time. The blue curve was recorded in the absence of Pt NPs.

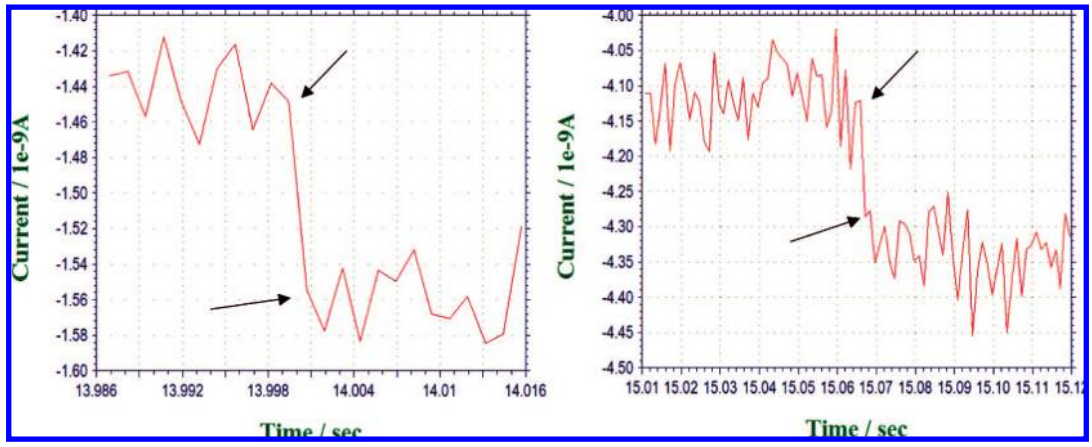


***Figure 3.*** High-temporal-resolution current transients for single Pt nanoparticle collisions. The data acquisition rate of the potentiostat was set at 1 ms. Particle size, ~3.6 nm; 10 $\mu$m Au UME; 15 mM hydrazine + 50 mM PBS buffer, pH ~7.5.

current amplification at Pt NPs. The application of single MNP collisions to determine particle size will also be discussed in the subsequent sections.

**Hydrazine Oxidation.** Figure 2 shows a representative current−time curve recorded at a Au UME, held at a potential of 0.1 V after mechanical polishing and electrochemical cleaning. The background current was about 220 pA and was essentially constant, decaying very slowly with time (Figure 2A, blue curve). The large noise observed from 5 to 15 s was caused by the opening and closing of the Faraday cage door while the Pt particle solution was injected. The current was slightly offset after that period, which might be due to one or a few particle collisions during this time period. Following this period, the solution was maintained as vibration-free as possible and the current monitored. As shown, the current increased anodically in a stepwise fashion. During the initial time period (Figure 2B), a few current steps of <20 pA in current amplitudes appeared. Note that these small current steps were also frequently observed later. Most of the current steps after this period were in the range of 40−65 pA. In each current step, the current increased very rapidly and then remained at a steady-state value. Figure 3 shows two typical current transients recorded at 1 ms time resolution. The risetime is within 1 ms. By using a higher time-resolution oscilloscope (Tektronix 2440) directly connected to the potentiostat, we found that the risetime of the current steps was about 40−100 $\mu$s. This risetime probably also is affected by the instrumental limits of the potentiostat. A few current steps showed longer transient times (Figure 2, blue arrows), which may indicate microscopic details about the nature of the particle collision with the substrate (Figure 2C), but this effect was not investigated further. For example, although improbable at low concentrations, a particle might collide and interact with another particle already on the surface. The rearrangement or fusion of two separate particles to become one unit would also lead to a decrease of practical surface area compared to that of the two separate NPs and thus show a relatively smaller electrocatalytic current. The MNP might also be deactivated by adventitious impurities in the solution. We have noted decays in the current, generally at longer recorded times. There are clearly subtleties in the detailed

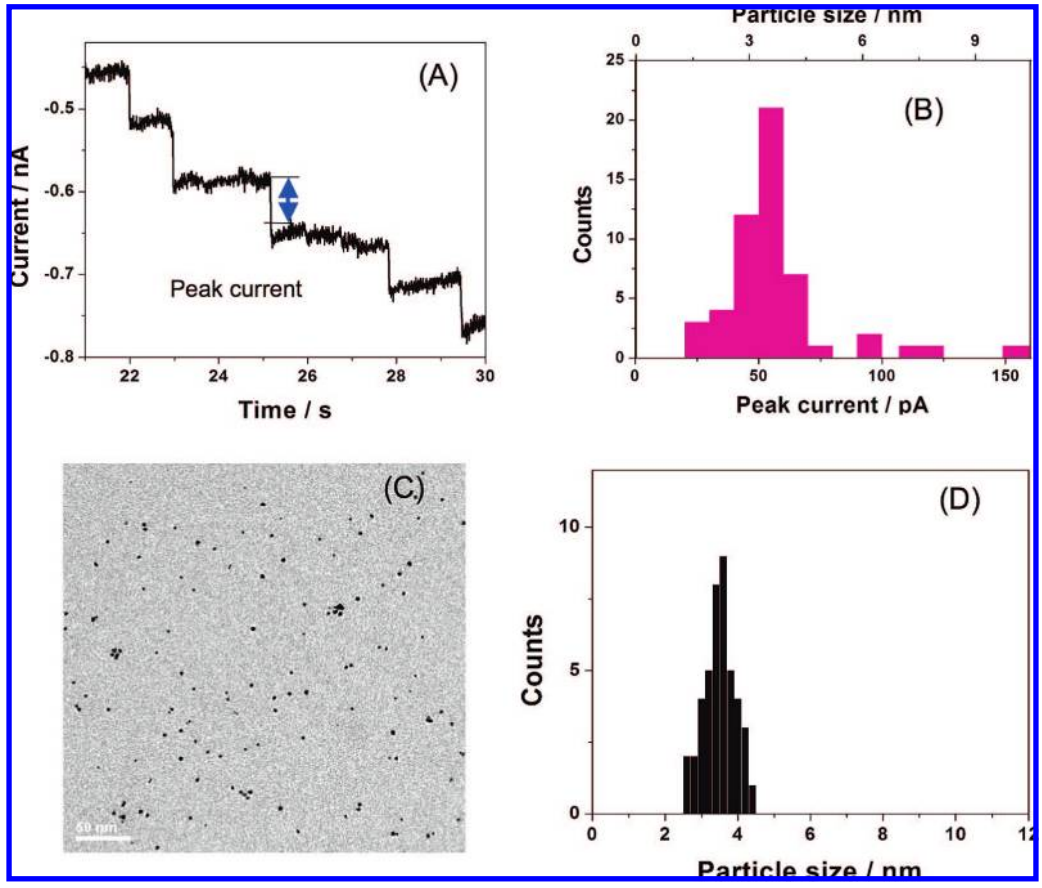


***Figure 4.*** (A) Representative current steps from Figure 2A. (B) Statistical peak current vs peak frequency analyzed for a 200 s interval. (C,D) TEM image and size distribution of the corresponding Pt nanoparticles.

shapes of the collision steps, which need to be studied further, but these are difficult to control.

Figure 4A shows a typical current vs time profile, which contains several steps of about equal height (~60 pA). This yields the particle radius via eq 1. For a larger number of steps one can plot the number of occurrences of a given peak current which indicates the main distribution between 40 and 65 pA, with smaller numbers of larger peak currents around 100 and 160 pA (Figure 4B). Since each current step profile signals a single particle collision event, the distribution of the peak currents should reflect the distribution of the NP sizes. Indeed, this agrees well with the particle size distribution determined by TEM (Figure 4C,D) by assuming that the size distributions of Pt NPs attached to the electrode and the TEM grid are similar, since in both cases Pt NPs are attached to the surfaces through particle random collision processes. The size distribution of MNPs should represent the particles attached at the electrode surfaces in the collision experiments described above. The larger peak currents are probably caused by collisions of MNP aggregates.

We confirmed that the individual current profiles are due to single MNP collisions by carrying out experiments under different experimental conditions, e.g., hydrazine concentration, particle concentration, nature and area of the detection electrode (C and Au UMEs), and the particle sizes. When the hydrazine concentration was changed, the amplitude of the current step changed proportionally for the same colloidal Pt solution injected (Figure 5). Therefore, for a given concentration of hydrazine, we can directly evaluate the particle size distribution by the distribution of peak currents. With increasing concentration of Pt NPs, the peak frequency was increased while the amplitude of the peak currents remained unaltered (Figure 6). The collision frequency was increased about twice when 25 $\mu$m diameter Au UMEs were used instead of 10 $\mu$m Au UMEs.

The first-order time derivative of the current was used to count steps and obtain the frequency of occurrence statistically, as shown in Figure 6B. Here, each spike represents a current step and thus a single particle collision event. The separation between individual spikes ranged from a few seconds to a few milliseconds. The large fluctuation in the frequency to observe spikes indicates that collisions of MNPs with the electrode from the bulk electrolyte are a random process. This collision process may also include some collisions of MNPs at the detector electrode, which do not lead to particle adsorption; i.e., the particle residence time at the electrode may be different from one particle to another. Many factors can affect the NP collision frequency, and we propose that not all collisions give rise to current steps, as discussed below.

The bronze (top) curve in Figure 6B shows the signal-to-noise level recorded in the absence of MNPs. The amplitude of the fluctuation is almost equally distributed in both upward and downward directions. The spikes having amplitudes larger than the ones indicated by blue arrows correspond to the current steps larger than 15 pA. These spikes are assigned to MNPs that stick to the substrate on collision. The average frequency of these spikes is about 0.012−0.02 $pM^{-1}$ $s^{-1}$ (i.e., for a 25 pM particle concentration, the frequency is about 0.4 $s^{-1}$, or an average time between collisions of about 2 s; Figure 6B, red curve). The spikes indicated by the red arrows might also be due to collisions of MNPs. Since these collisions lead to current spikes rather

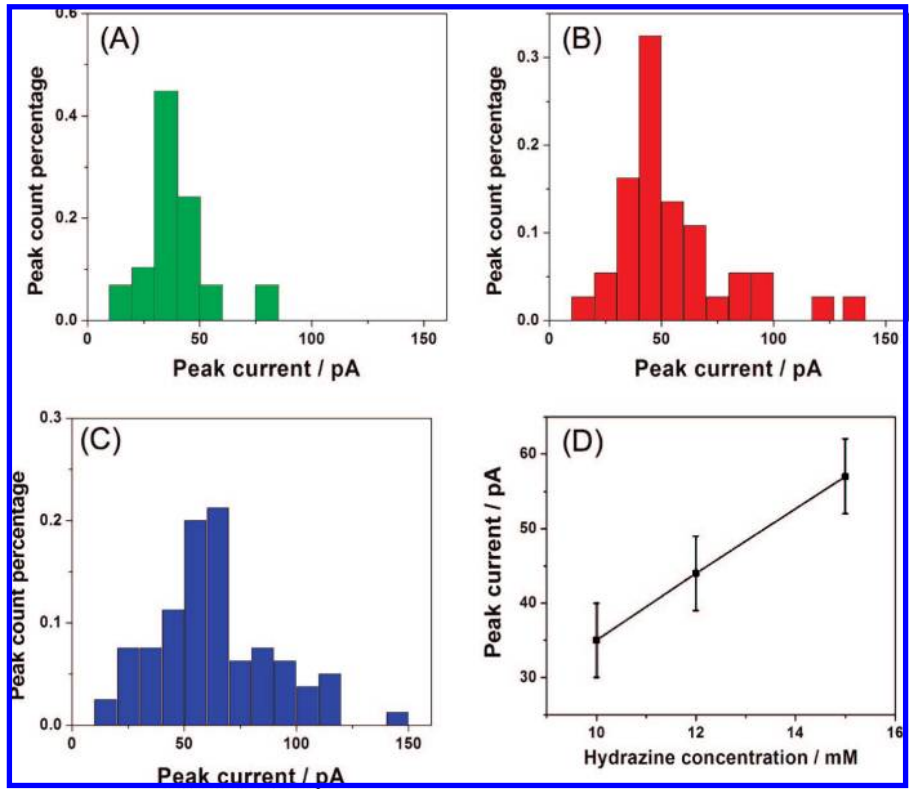


***Figure 5.*** (A−C) Statistical peak current distribution at three different hydrazine concentrations. Peak count percentage is defined as the number of peaks of a given peak current divided by the total number of peaks counted. (D) Plot of main peak current vs hydrazine concentration. The deviation of the current for each data point is about ±5 pA.

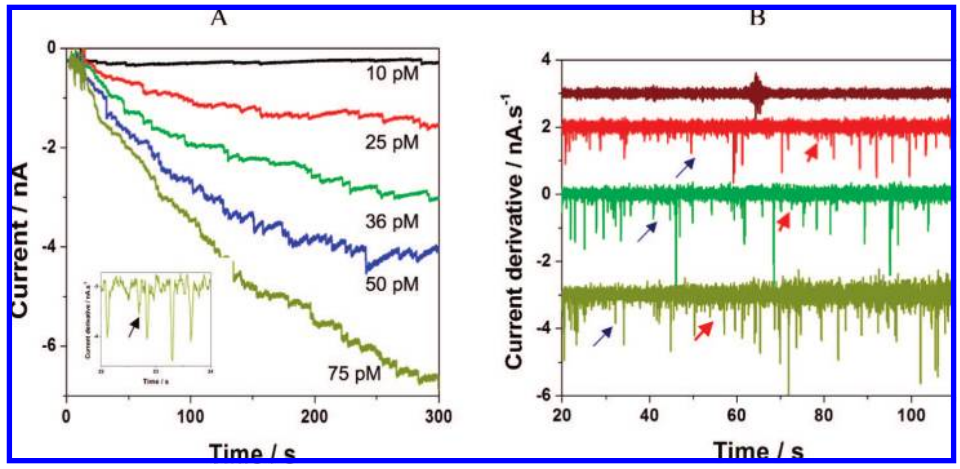


***Figure 6.*** (A) Current transients recorded at individual Pt particle concentrations and (B) the correspondent first-order derivatives. The bronze curve in (B) is the current transient recorded in the absence of MNPs. The traces are offset from zero for clarity. The blue arrows point to spikes, which give rise to current steps above 20 pA, and the red ones to the current steps less than 20 pA. Particle size, ∼3.6 nm; 10 $\mu$m Au UME; 15 mM hydrazine + 50 mM PBS buffer, pH ∼7.5.

than current steps, they may be caused by collisions of MNPs that have a very short residence time at the detection electrodes. The appearance of some consecutive collisions within a few milliseconds indicates that the particles might have already interacted with each other in the solution phase.

One can estimate the collision frequency by first assuming that all MNPs collide and stick at the detector electrode at diffusion-limited steady-state conditions, thus yielding a flux $J$, given by

$$J = 4D_pC_p/\pi a \qquad (2)$$

where $D_p$ and $C_p$ are the diffusion coefficient and concentration of Pt particles, and $a$ is the radius of the UME. This is the equation for the diffusion-controlled flux to an UME.[24] With a known particle concentration and radius of an Au UME, the observed collision frequency would correspond to a NP diffusion coefficient of $\sim 1 \times 10^{-8}$ cm$^2$/s.

However, the diffusion coefficient of Pt NPs in the range of 3−4 nm should be larger, $\sim 1 \times 10^{-7}$ cm$^2$/s based on the Stokes−Einstein relation for NP diffusion and also from experiments.[27,28] The reason $D_p$ is 10 times smaller than the value from eq 2 is probably that not all collisions (in fact, only

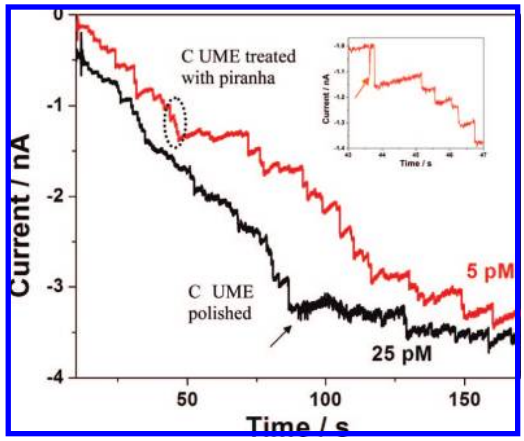


***Figure 7.*** Current transients recorded before and after injection of Pt NPs at a C UME polished (black) and further treated with piranha solution (red). Electrode potential, 0.5 V; Pt NP size, ~3.6 nm; test electrolyte, 15 mM hydrazine + PBS buffer. The inset curve shows a current spike followed by current steps.

about one in 10 to one in 100) result in particle sticking, but we have no direct evidence for this. In order for a current step to be observed, the particle has to stay in contact with, or at tunneling distance from, the electrode surface for a time long enough to generate observable current. While this could occur with a particle making multiple collisions with the electrode while in the "solvent cage" near the electrode, the fact that one sees a continuous staircase suggests that the particles recorded stick and remain on the surface. We observed very few current steps in the opposite direction, where a particle would leave the surface. Thus, what we observe is closer to the sticking frequency rather than the collision frequency.

We have found that many experimental parameters affect the sticking probability of MNPs. We observed a slight increase in sticking frequency when the potential of the detection electrode was set more and more positive. When the Au UME was covered by a 3-mercaptopropionic acid monolayer, the sticking frequency decreased slightly, while it remained almost the same when the surface was covered by a cystamine monolayer. At pH ~7.5, 3-mercaptopropionic acid made the surface negatively charged, and cystamine maintained the surface almost neutral, similar to a pure Au electrode. These experiments suggest that an electrostatic interaction between the charged surface and the charged particles may play a role in the particle sticking probability. However, the frequency change among these different surfaces was relatively small, no more than a factor of 2. We did find about a 5 times or greater increase in sticking frequency after the C electrode was treated by piranha solution. As shown in Figure 7, the frequency increased to be almost the same for a C electrode treated by piranha solution with a particle concentration of 5 pM as for an untreated electrode with a 25 pM particle concentration. The piranha-treated electrode also showed fewer current spikes, indicated by the arrows, compared to an untreated one, indicating that Pt NPs stick better after piranha treatment, since such current spikes represent short residence collisions. The increase in sticking probability indicates that the nature of the surface is important. It might indicate a surface hydrophobicity change, since after piranha treatment the C surface becomes more hydrophilic. Particles might also stick in minute cracks and defects on the surface, the number of which is increased by the treatment.

Note also that the number of particles counted on TEM grids (carbon covered Cu), such as those shown in Figure 4C, when the grid was simply immersed in the MNP solution for a given time and then removed, is also much smaller than that calculated from eq 2 and was seen to vary from place to place on the grid. For a TEM sample immersed in a 25 pM Pt colloidal solution overnight, we would estimate >1000 particles/$\mu m^2$ by eq 2, using a diffusion coefficent of $1 \times 10^{-7}$ $cm^2/s$. In fact, we could not find any area of the surface with this density of MNPs. Instead, many surface areas had <20 particles/$\mu m^2$. The smaller number of particles observed at the TEM grids suggests a poor sticking property of Pt NPs after collision with these surfaces, as was found with our electrodes.

**Proton Reduction.** Proton reduction at carbon electrodes occurs sluggishly and requires a high overpotential, while this reaction is rapid at Pt, as demonstrated by cyclic voltammograms at Pt and C UMEs in strong and weak acid electrolytes (Figure 8A). A steady-state diffusion-limited current was observed in both $HClO_4$ and sodium dihydrogen citrate ($NaH_2Cit$). In the collision experiments, we used 50 mM $NaH_2Cit$ as the proton source since Pt NPs are relatively stable in this environment, while they tend to aggregate in 5 mM $HClO_4$. The steady-state limiting current is about 70 nA at a 10 $\mu$m Pt UME. Injection of a Pt NP colloidal solution to 100 mM $NaH_2Cit$ or pure $HClO_4$ leads to aggregates. Figure 8B shows three current−time curves recorded at carbon fiber microelectrodes. No obvious current spikes were observed either in the background experiment or when a solution of C NPs (instead of Pt NPs) was injected into the test electrolyte. The C NP solution was made from carbon black (Vulcan XC72R). When Pt NPs were injected, the overall current increased, superimposed with current spikes. These current spikes are similar to those observed in the case of hydrazine oxidation. However, the current did not maintain a constant steady-state level for times as long as those observed with hydrazine oxidation. The current remained at the maximum value for only <1 s and then decayed slowly almost to the background level (Figure 8C,D). Note that almost every current profile showed such a current decay. The peak currents ranged from 30 to 80 pA, which corresponds to a particle size of about 4 nm.

Since the decay of the current following a collision is more prominent with proton reduction than with hydrazine oxidation, we examined current transients at Pt UMEs for proton reduction and hydrazine oxidation and compared them to ferrocene−methanol oxidation. The current transient for ferrocene−methanol oxidation shows a negligible current decay after reaching the steady-state current within 20 ms (Figure 9A). Hydrazine oxidation shows behavior similar to that of ferrocene−methanol (Figure 9B), while proton reduction shows a slightly longer transient time, especially at the carbon electrode modified with Pt NPs (Figure 9C). From 0.5 to 10 s, the current decayed about 6% for ferrocene−methanol, 3% for hydrazine, and 32% for proton (Figure 9C, blue). From 10 to 20 s, the current decay was about 1% for both ferrocene oxidation and hydrazine oxidation, and 5% for proton reduction. The small difference at a long polarization time suggests that the current decay is mainly due to progressive surface contamination. The progres-

(27) Hicks, J. F.; Zamborini, F. P.; Osisek, A.; Murray, R. W. *J. Am. Chem. Soc.* **2001**, *123*, 7048–7053. Chen, S. W.; Ingram, R. S.; Hostetler, M. J.; Pietron, J. J.; Murray, R. W.; Schaaff, T. G.; Khoury, J. T.; Alvarez, M. M.; Whetten, R. L. *Science* **1998**, *280*, 2098–2101.

(28) Wada, Y.; Totoki, S.; Watanabe, M.; Moriya, N.; Tsunazawa, Y.; Shimaoka, H. *Opt. Express* **2006**, *14*, 5755–5764.

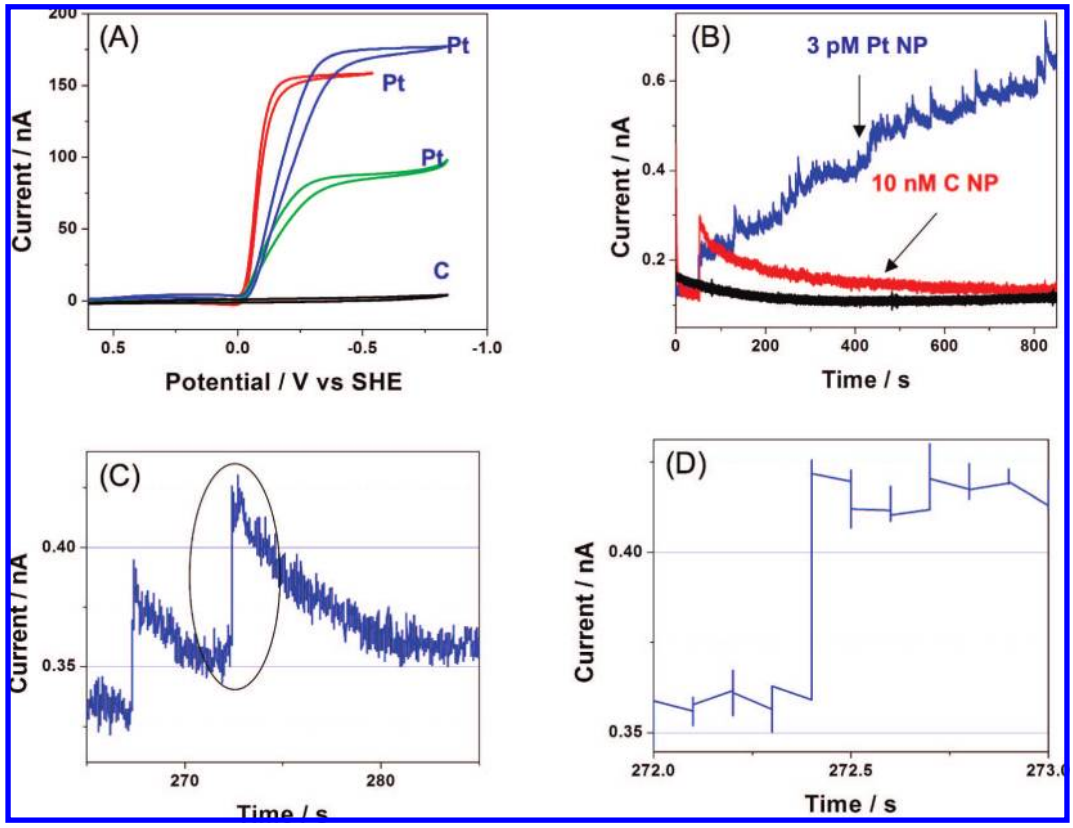


***Figure 8.*** (A) Cyclic voltammograms at Pt and C UMEs in 50 and 100 mM sodium dihydrogencitrate electrolytes (green and blue) and 10 mM perchloric acid electrolyte (red), 100 mV/s. (B) Current transients recorded before (black) and after injection of C (red) and Pt (blue) nanoparticle solutions. (C,D) Zoom of individual current profiles. 50 mM sodium dihydrogen citrate; electrode potential, −0.5 V; Pt nanoparticle size, ∼3.6 nm; C nanoparticle size, ∼25 nm; detection electrode, C UME of 10 $\mu$m diameter.

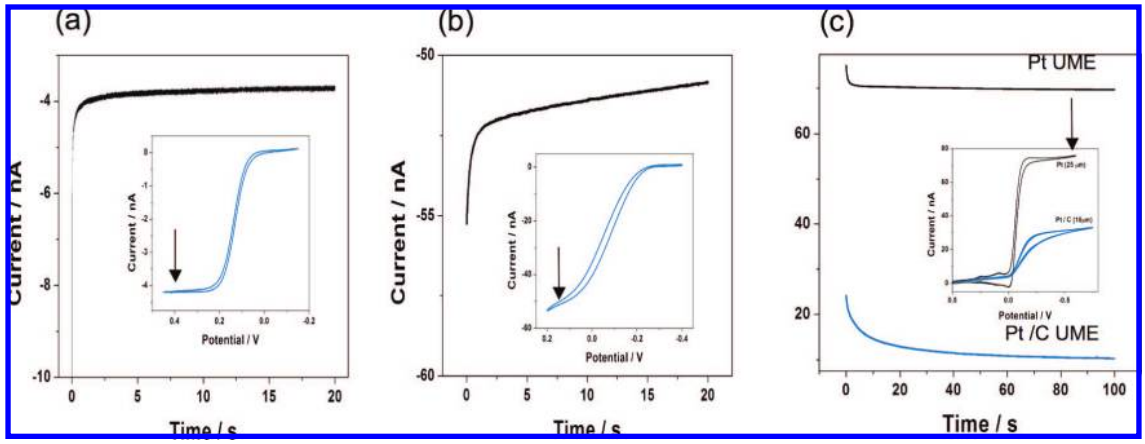


***Figure 9.*** Current transients and cyclic voltammograms at Pt UMEs in (A) ∼3 mM ferrocene−methanol + 0.1 M sodium perchlorate, (B) 12 mM hydrazine + 50 mM PBS buffer, and (C) 2 mM perchloric acid + 20 mM sodium perchorate. The black arrows indicate the pulse potentials. (A,B) Pt, 10 $\mu$m diameter; (C) Pt, 25 $\mu$m (black) and Pt deposited at carbon fiber, 8 $\mu$m in diameter (blue).

sive surface contamination could also lead to current decrease in successive potential pulses. In the case of hydrazine oxidation, we found that the current decay is more severe at Pt UMEs than at Au UMEs. The surface contamination at MNPs may be worse than that at macroelectrodes because of their high relative surface area and the higher mass-transfer rates of trace impurities to nanometer-size centers. This would be especially important for the hydrogen evolution reaction that depends upon adsorption of hydrogen atoms on Pt. Another mode that could cause current decay is the adsorption of hydrogen atoms into the lattice of the Pt MNPs. Pletcher[29] noted deactivation of a Pt UME and proposed this as a possible cause.

We have observed a similar current decrease at the Pt UME when the concentration of phosphate was increased to 200 mM, indicating that the current decay was not due to the low concentration of supporting electrolyte (used to favor the stability of MNPs). However, the current decay was smaller at Au UMEs, which suggests that the current decay is probably related to the catalytic properties of Pt surface.

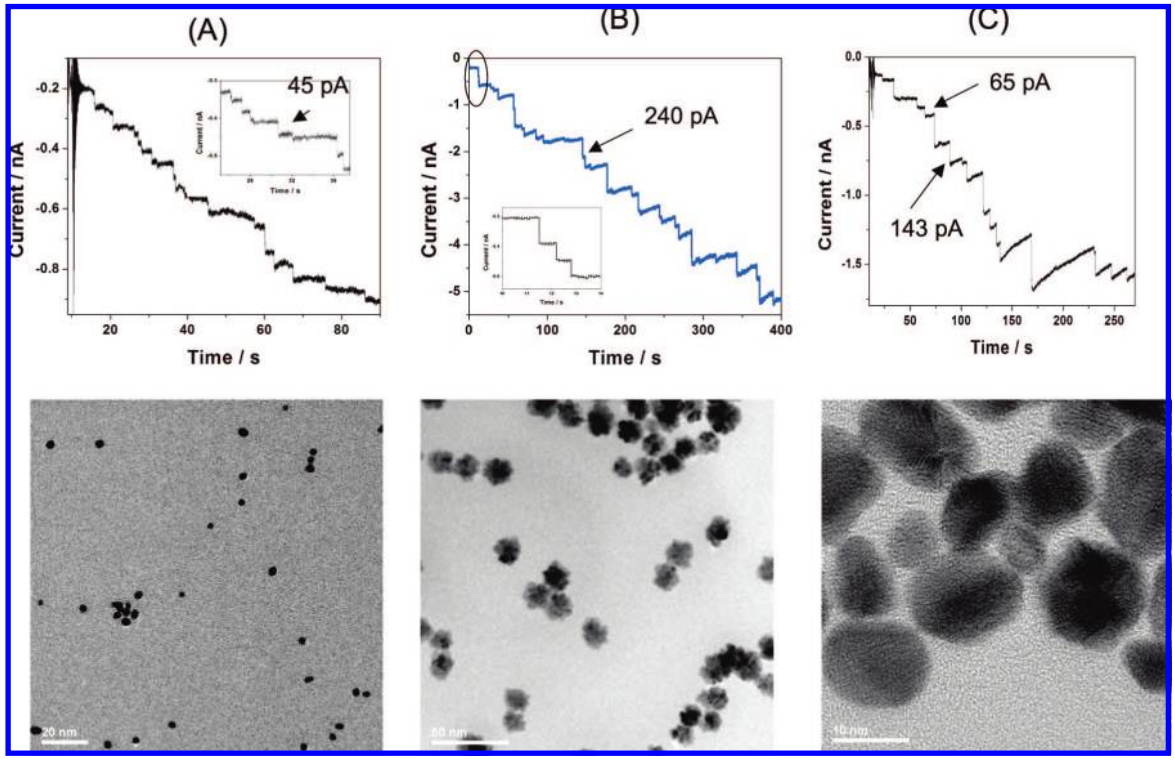


***Figure 10.*** Current transients recorded for individual Pt nanoparticles of different particle sizes. The TEM images of the correspondent Pt NPs are shown underneath, respectively. The concentration based on Pt atoms is about (A) 50, (B) 500, and (C) 250 nM. Ten micrometer Au UME; 12 mM hydrazine + 50 mM PBS buffer, pH ~7.5.

**Application of Single Nanoparticle Collisions To Determine Particle Size Distributions.** The above results indicate that each current profile is a signature of single MNP collisions at the electrode. We have proved this further by varying the size of Pt NPs. The particle sizes and size distribution could be also determined from the corresponding current profiles. Figure 10 shows representative current transients recorded for several Pt colloidal solutions with different particle sizes. Since the Pt NPs were stabilized by similar capping molecules, citrate or oxalate, we assume that they have similar catalytic properties. When these NP solutions were injected into the hydrazine test electrolyte, the recorded current transients showed discrete current steps of very different current amplitudes. For ~3.6 nm Pt NPs, the current steps had almost uniform amplitude which was mainly distributed around 45 pA (Figure 10A). In the case of star-like Pt NPs (Figure 10B), the peak currents were mainly distributed around 240 pA, corresponding to a particle size of about 20 nm. A small fraction of current peaks had peak currents smaller than ~120 pA or larger than ~300 pA, probably due to the existence of some small particles and aggregates of two to three units. Figure 10C shows the current transient recorded for polydisperse Pt NPs. The peak currents were distributed over a wide range between 60 and 200 pA, corresponding to particle sizes ranging from 5 to 16 nm. The amplitudes of the peak currents for the cases studied seem to correlate well with the particle size distribution found by TEM. This suggests that any sticking probability is essentially independent of particle size.

## Conclusions

Electrocatalytic amplification allows the observation of single MNP collisions, characterized by individual current steps generated when the Pt NPs collide and stick to the detector electrode. The current flows when the MNPs switch on an electrocatalytic reaction at their surfaces at a potential where the detector electrode shows negligibly small electrochemical activity. The observed current profiles during each collision are similar to current transients recorded at UMEs and are a function of the NP radius. The kinetics of the electrocatalytic reactions play an important role in the observed current and the usefulness of this technique for studying the kinetics of electrocatalysis at the nanometer scale.

At mass-transport-controlled conditions, the amplitude of each current step is correlated to the particle size. A plot of the current amplitudes versus the frequency of peak occurrence correlates well with the particle size distribution as found with TEM, thus providing an electrochemical approach to the rapid screening of NP dispersions. Since the collision frequency is also correlated to the effective surface area of the detector electrode, this technique may be useful in evaluating the porosity of insulating films at electrode surfaces.

**Acknowledgment.** We appreciate valuable discussions with Drs. S. Feldberg, R. M. Crooks, and C. Zoski. We also acknowledge support from the National Science Foundation (CHE 0451494 and CHE 0808927).

JA8051393

(29) Pletcher, D. In *Microelectrodes: Theory and Application*; Montenegro, M. I., Queirós, M. A., Daschbach, J. L., Eds.; Kluwer Academic: Dordrecht, 1991; p 472.